

EFFECT OF Fe DOPANT ON PHYSICAL PROPERTIES OF ANTIMONY SULPHIDE (Sb₂S₃) THIN FILMS

Z. U. ABDIN^a, M. H. ALNASIR^b, M. Y. KHAN^{c*}, M. SAJJAD^c,
M. T. QURESHI^d, A. ULLAH^e, A. ZEB^a

^a*Department of Applied Physics, Federal Urdu University of Arts, Science and Technology, Islamabad 44000, Pakistan*

^b*Department of Physics, COMSATS University, Islamabad 44000, Pakistan*

^c*Department of Physics, Kohat University of Science and Technology, Kohat 26000, Pakistan*

^d*Department of Physics, Hazara University, Mansehra 21300, Pakistan*

^e*Department of Physics, University of Science & Technology, Bannu 28100, Pakistan*

Iron (Fe)-doped antimony trisulphide (Sb₂S₃) thin films were prepared by Chemical Bath Deposition (CBD) technique at temperatures 0 °C, 5 °C and 10 °C for 4 h and were annealed at 500 °C for 2 hours under N₂ environment. The crystallinity and morphology of un-doped and Fe-doped Sb₂S₃ thin films was studied with X-Ray Diffraction (XRD) and Scanning Electron Microscope (SEM), respectively. Chemical composition as well as thickness of the thin films was determined by Rutherford Back Scattering (RBS) spectroscopy. UV-Vis spectroscopy revealed that for un-doped and Fe-doped Sb₂S₃ thin films the optical band gap values increase to lie within the photoactive-visible region making them suitable for solar cell applications.

(Received November 25, 2018; Accepted January 15, 2019)

Keywords: Antimony trisulphide, Chemical bath deposition, Thin films, Structural properties, Optical band gap

1. Introduction

Antimony trisulphide (Sb₂S₃) thin films are being studied from the last two decades due to their attractive photosensitivity, thermoelectric properties, high refractive index, large dielectric constant, thermoelectric semiconductor and well-defined quantum size [1-4]. In addition to low toxicity, Sb₂S₃ has a band gap of 1.6 to 2.5 eV, which covers visible and infrared region of solar system [5-8]. These films also have high absorption coefficient (10⁴ - 10⁵ cm⁻¹) [9] making them suitable for optoelectronic and solar thermal devices such as semiconductor sensitized solar cell, Schottky diodes, photoanode material in photocatalytic water splitting, thin film photovoltaics and solar cells yielding power conversion efficiency of 6.5% etc. [10-14].

During recent past Si solar cells gained much attention due to their abundance, non-toxicity, high and stable cell efficiencies [15], but cannot overcome the energy crises due to their high cost [16]. Different materials such as SbSn, GaAs, InGaAs, AlGaAs, and TiO₂ have been reportedly used to obtain optoelectronic properties [17, 18]. Efforts have been made to choose low-cost materials with direct band gap and absorb more light [19]. For this purpose, Sb₂S₃ thin films are considered to be potential candidates. Sb₂S₃ has high resistivity, which restricts their use in photovoltaics. So far, few attempts have been made to enhance the structural, optical and electrical properties by doping different elements like Sn, Ni, C, Ag having less or extra electrons in their valence shell as compared to host fragments which affect the resistivity of the material [16, 20-24]. Ag-doping in Sb₂S₃ at different positions not only decreases their resistivity, but also increases their refractive index [25].

Till now, different techniques have been employed to prepare doped and un-doped Sb₂S₃ thin films such as three temperature method, vacuum evaporation, chemical bath deposition, two-

* Corresponding author: yaqoobkhattak@hotmail.com

stage process, rapid thermal process, spray pyrolysis, hydrothermal deposition method etc. Chemical Bath Deposition (CBD) technique is known for its low-cost at low temperatures and is suitable for deposition of large area thin films. Many researchers investigated Sb_2S_3 thin films preparation using CBD [26-28]. Different film preparation techniques also affect the band gap energy value. Savadogo and Mondal reported 1.8 eV band gap energy for Sb_2S_3 thin films by using CBD technique [11]. Spray pyrolysis technique is used by Bhosale *et al.* [9], and they reported band gap energy 1.55 eV. Later, Yesugade *et al.* investigated Sb_2S_3 , As_2S_3 , and Bi_2S_3 by using Electro Deposition Technique and reported 1.7 eV energy for the band gap of Sb_2S_3 [29].

In the present work, we have reported Fe-doped Sb_2S_3 thin films with Fe concentration of 1 %, 2 %, 3 % and 4 % prepared by CBD method at three different temperatures i. e., 0 °C, 5 °C and 10 °C. The structural, morphological and optical and properties of un-doped and Fe-doped Sb_2S_3 films were studied using X-ray diffraction (XRD), scanning electron microscopy (SEM), energy-dispersive X-ray spectroscopy (EDS) and UV-Vis spectroscopy. In our study, the optimal band gap was found to be in the range 1.53 – 1.97 eV. The bath temperature was also optimized and its value for best synthesis of the under study films was found to be 10 °C.

2. Experimental procedures

2.1. Preparation of antimony trisulphide (Sb_2S_3) thin films

Glass substrate was used in this work to prepare the pure and Fe-doped Sb_2S_3 thin films. The glass substrate (75 mm length, 25 mm width, and 1 mm thickness) was cleaned well in soap solution with a cotton piece, then was rinsed with distilled water and further etched with 5% of hydrochloric acid (HCl) for 30 minutes and then cleaned ultrasonically. The cleaned glass substrate was put in a vacuum oven for half an hour. The solution was prepared according to a procedure published elsewhere [16, 30]. The chemical bath was prepared by dissolving 650 mg of Antimony trichloride (SbCl_3) in 10 ml acetone, and 25 ml of a 1M solution of sodium thiosulphate ($\text{Na}_2\text{S}_2\text{O}_3$) in 65 ml distilled water, and further; both solutions were mixed in a beaker. Resultantly, the whole mixture becomes transparent. The mixed solution was stirred well, and was turned into orange color after 10 to 15 minutes. For the deposition of Sb_2S_3 films, the clean glass substrate was placed vertically in the beaker solution for 4 h, and the bath temperature was kept at 0 °C, 5 °C and 10 °C respectively. A thermometer and magnetic stirrer were placed in the beaker at the same time. The pH of the prepared solution was increased from 1.5 to 3.5 after mixing. The Sb_2S_3 thin film was deposited on both sides of the glass substrate. Gently, the glass substrate was placed horizontally on the table after cleaning one side of it with cotton swabs moistened with dilute HCl (1%) [30]. At the end, films were washed with distilled water and dried under N_2 flow. To avoid any oxidation, the films were annealed for 4 h at 500 °C under N_2 flow. The prepared thin films were placed in the glove box to avoid contamination. The Sb_2S_3 formation mechanism first involve the formation of $\text{Sb}_2(\text{S}_2\text{O}_3)_3$ from SbCl_3 and $\text{Na}_2\text{S}_2\text{O}_3$ [6, 31], which turned to be hydrolyzed to form Sb_2S_3 . The Sb^{3+} and $(\text{S}_2\text{O}_3)^{2-}$ ions also produced through decomposition of intermediate $\text{Sb}_2(\text{S}_2\text{O}_3)_3$ whereas the hydrolysis of $(\text{S}_2\text{O}_3)^{2-}$ ions reacts with water to produce S^{2-} ions which react with Sb^{3+} ions to form a Sb_2S_3 thin film [22]. For the preparation of Fe-doped Sb_2S_3 thin (Sb_2S_3)_(100-x)Fe_x, ferrous chloride powder (99 % pure powder) was dissolved by varying the Fe percentage concentration (1 %, 2 %, 3 % and 4 %) into the antimony trisulphide solution with percentage concentration of 99%, 98%, 97% and 96%, respectively. The rest of the experimental parameters were kept similar as described earlier. All the Fe-doped thin films were prepared at 10 °C for 4 h and were annealed at 500 °C for 2 h under N_2 flow to improve crystallinity.

2.2. Characterization

Siemens X-Ray diffractometer was used to observe crystal structure of the prepared (doped and un-doped) thin films with Cu K α radiation ($\lambda = 1.542\text{\AA}$). The scanning range was 20° - 960° at 40 kV and 40 mA. The surface morphology and composition of doped and un-doped Sb_2S_3 thin films with size 1 cm \times 1 cm, was analyzed using SEM (model: JEOL JSM-63602LV) equipped with EDX. To study the influence of dopant on the composition of the layers, the Rutherford Back Scattering (RBS) techniques were used, using 2MeV He^{2+} ion beam operating at

20 keV for compositional analyses. UV-Visible spectrometer (Perkins Elmer Lambda - 25) was used to measure the optical constants such as optical absorption coefficient and energy band gap etc. in the range of 400 -800 nm.

3. Results and discussion

3.1. X-ray diffraction analysis

The X-ray diffraction patterns were obtained for pure and Fe-doped Sb_2S_3 thin films synthesized using CBD on glass substrates at different temperatures. The 2θ range was from 0° to 60° for all XRD measurements. Iron was doped in Sb_2S_3 thin films that were deposited at 10°C and annealed at 500°C under N_2 flow. All XRD patterns are shown in Fig. 1. Annealing of the prepared films at 500°C results in XRD peaks that show high crystallinity as compared to the unannealed films (not shown here). All the values for 2θ and d - spacing of the respective diffraction peaks for Fe-doped and un-doped Sb_2S_3 films revealed an orthorhombic structure. The (200), (220), (310), (121), (221), (231), (341) and (061) peaks observed at $2\theta = 16.01, 22.44, 24.99, 29.22, 32.25, 37.08, 46.91$ and 54.26 respectively matched with the standard pattern. Identification of peaks were made using Stibnite phase ICSD # 00-002-0374. No extra peaks have been observed which confirms the fact that Fe has been substituted in the Sb_2S_3 lattice. No peak corresponding to Fe was detected. In addition, the intensity of peaks decreases in the Fe doped samples along with increment in the full width half maximum (FWHM) which is due to the lower crystallinity of the doped samples compared to the un-doped Sb_2S_3 as shown in Fig 1 (b). The shift of peaks to the larger angles reflects the lattice distortion and lattice defects in Sb_2S_3 unit cell which shows that size of dopant is larger as compared with the Sb^{+3} . This suggests that Fe doping causes a reduction in doped films planes. Similar results have been reported by other researchers [20, 25, 30, 32].

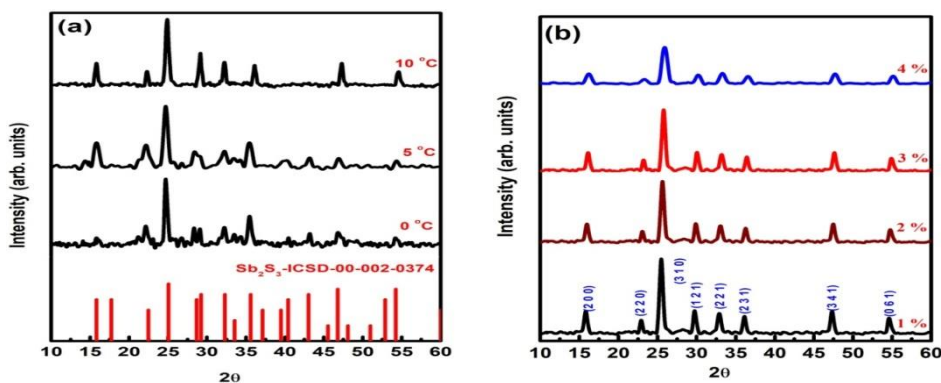


Fig. 1. A representative powder X-ray diffraction pattern of (a) pure Sb_2S_3 thin films prepared by chemical bath deposition technique at 0°C , 5°C , and 10°C and the calculated PXRD pattern of Sb_2S_3 (red). (b) Doped $(\text{Sb}_2\text{S}_3)_{(100-x)}\text{Fe}_x$ thin films for $x = 1, 2, 3, 4$.

Several parameters, i.e., crystallite size, dislocation density, lattice strain and lattice parameters for un-doped and Fe-doped Sb_2S_3 thin films were calculated to get information about the microstructure of the thin films. The average grain size $\langle D \rangle$ can be estimated from the broadening of three peaks (200), (310) and (121) using the Scherrer's equation:

$$D = \frac{0.9\lambda}{\beta \cos\theta}$$

where $\lambda = 1.542 \text{ \AA}$ is the X-ray wavelength, β is the FWHM and θ is the Bragg's angle.

The lattice constants, “ a ”, “ b ”, and “ c ”, were determined for un-doped and Fe-doped Sb_2S_3 films using the following relations [33]:

$$\frac{1}{d^2} = \frac{h^2}{a^2} + \frac{k}{b^2} + \frac{l^2}{c^2}$$

The dislocation density “ δ ”, due to Fe addition was calculated using:

$$\delta = \frac{1}{D^2}$$

The lattice strain “ ε ” was calculated for un-doped and Fe-doped Sb_2S_3 thin films using:

$$\varepsilon = \frac{\beta}{\tan\theta}$$

The volume unit cell volume “ V ”, and X-ray density “ ρ ” were determined using:

$$V_{cell} = \frac{abc}{ZM}$$

$$\rho = \frac{ZM}{N_A V_{cell}}$$

where N_A is the Avogadro number also calculated using Bragg’s relation, Z is the number of molecules in formula unit, M is the molar mass.

The texture coefficient $TC(hkl)$, was calculated for main planes using:

$$TC(hkl) = \frac{\frac{I(hkl)}{I_o(hkl)}}{\sum_N \frac{I(hkl)}{I_o(hkl)}} N$$

where $I_o(hkl)$ is the standard plane intensity, $I(hkl)$ is the observed intensity and N is the no of peaks to be considered.

Table 1 shows the microstructural parameters calculated for un-doped Sb_2S_3 thin films developed at different temperatures. The average crystallite size of Sb_2S_3 thin films heat-treated at 0°C , 5°C and 10°C was found to be 31 nm, 27 nm, and 18 nm respectively, while crystal strain was found to increase from 1.05×10^{-3} to 2.96×10^{-3} at higher temperatures with the decrease of crystallite size. The lattice parameter “ a ” of un-doped Sb_2S_3 unit cell is found to be increased from 10.22 Å to 11.22 Å, while the lattice parameters “ b ” and “ c ” are found to be decreased with the increase of temperature.

Table 1. Microstructural parameters calculated from XRD patterns of un-doped Sb_2S_3 thin films at different temperatures.

	Sb_2S_3^*	0°C	5°C	10°C
a (Å)	11.2	10.22	10.86	11.22
b (Å)	11.28	11.95	11.49	11.25
c (Å)	3.83	4.83	4.01	3.85
V_{cell} (Å) ³	484	589	500	486
ρ (g/cm ³)	4.66	3.83	4.51	4.64
D (nm)		31	27	18
δ (nm ⁻²)		1.05×10^{-3}	1.40×10^{-3}	2.96×10^{-3}
ε		1.35	1.55	2.25

* Standard values

The calculated values of lattice and microstructural parameters for un-doped and Fe-doped Sb_2S_3 are tabulated in Table 2. Crystallite size for the Fe-doped films is found to decrease from 16 nm to 9 nm, whereas the crystal strain increases from 2.96×10^{-3} to 13.94×10^{-3} and the lattice strain increases from 2.25 to 4.79 due to the large ionic size of Fe which leads to the growth of smaller crystallite size of Sb_2S_3 . It is also observed that lattice constants “a” and “b” were found to be increased while that of “c” was found to be decreased with the increase of Fe-dopant concentration.

Table 2. Microstructural parameters calculated from XRD patterns of un-doped and Fe-doped Sb_2S_3 thin films (Sb_2S_3)_(100-x)Fe_x.

	$Sb_2S_3^*$	0%	1%	2%	3%	4%
a (Å)	11.2	11.22	11.27	11.1	11.5	11.7
b (Å)	11.28	11.25	11.35	11.38	11.42	11.62
c (Å)	3.83	3.85	3.84	3.75	3.71	3.65
V_{cell} (Å) ³	483.87	485.97	491.19	473.69	487.23	496.23
ρ (g/cm ³)	4.66	4.64	4.21	3.97	3.47	3.03
D (nm)		18	16	14	12	9
δ (nm ⁻²)		2.96×10^{-3}	3.99×10^{-3}	5.40×10^{-3}	6.96×10^{-3}	13.14×10^{-3}
ε		2.25	2.62	3.04	3.47	4.79

* Standard values.

The Texture Coefficient (TC) was calculated from intensity ratio of respective planes for un-doped and Fe-doped Sb_2S_3 films [30] and is shown in Table 3. The result shows that un-doped and 1 – 2% Fe-doped Sb_2S_3 along (310) plane, and 3 – 4% Fe-doped Sb_2S_3 along (221) and (341) planes are highly textured showing a higher degree of preferred orientation along particular plane(s). There is a decrease in TC along (310) plane for Fe-doped samples showing deviation in texture coefficient from unity, while the Fe-doped films show a significant increase in TC along (221) and (341) planes due to increase in planar density [34]. Therefore, the addition of Fe in Sb_2S_3 lattice creates vacancies along (310) plane and there is an increase in planar density for (221) and (341) planes of Sb_2S_3 unit cell.

Table 3. Texture Coefficient (T_c) for un-doped and Fe-doped Sb_2S_3 thin films.

Planes (hkl)	Texture coefficient				
	Un-doped Sb_2S_3		Fe-doped Sb_2S_3		
	0%	1%	2%	3%	4%
(310)	1.062	1.053	1.025	0.947	0.923
(221)	0.975	0.953	0.961	1.001	1.015
(341)	0.963	0.986	1.022	1.052	1.061

3.2. SEM and EDX analysis

The morphology of un-doped samples of Sb_2S_3 prepared at 0 °C, 5 °C and 10 °C was studied using scanning electron micrographs (SEM), and the obtained images are shown in Fig. 2. The un-doped Sb_2S_3 films prepared at different temperatures show aggregated, unevenly distributed, interconnected surface particles all over the surface, which does not affect peaks formation and is similar to the reported work [7, 30, 35]. The Sb_2S_3 thin films prepared at 0 °C and 5 °C have grains of spherical shapes with diameter of around 30 - 33 nm and 26 - 30 nm respectively, while those prepared at 10 °C have spherical diameter around 15 - 20 nm. The sizes observed using SEM images match with the size determined through XRD.

In order to confirm the composition of un-doped Sb_2S_3 thin film prepared at 0 °C, 5 °C and 10 °C, an energy dispersive X-ray (EDX) spectrum was obtained. The peaks obtained from EDX spectrum (Fig. 2) shows that “Sb” and “S” elements are present in the prepared thin films. The results show that films are highly stoichiometric, whereas the peaks corresponding to “Na” and “Si” are due to the glass substrate and “Cl” peaks are due to the Antimony trichloride ($SbCl_3$) [36]. No oxygen peak was observed for un-doped thin films and is similar to the reported work [27, 36], but this peak is observed for Fe-doped Sb_2S_3 (not shown here). Un-doped Sb_2S_3 thin film prepared at 0 °C shows that atomic percentage of “Sb” is smaller than that of “S”, and this percentage increases by raising bath temperature from 5 °C, and 10 °C. These results are in agreement with the ones obtained through XRD as given in Table 1.

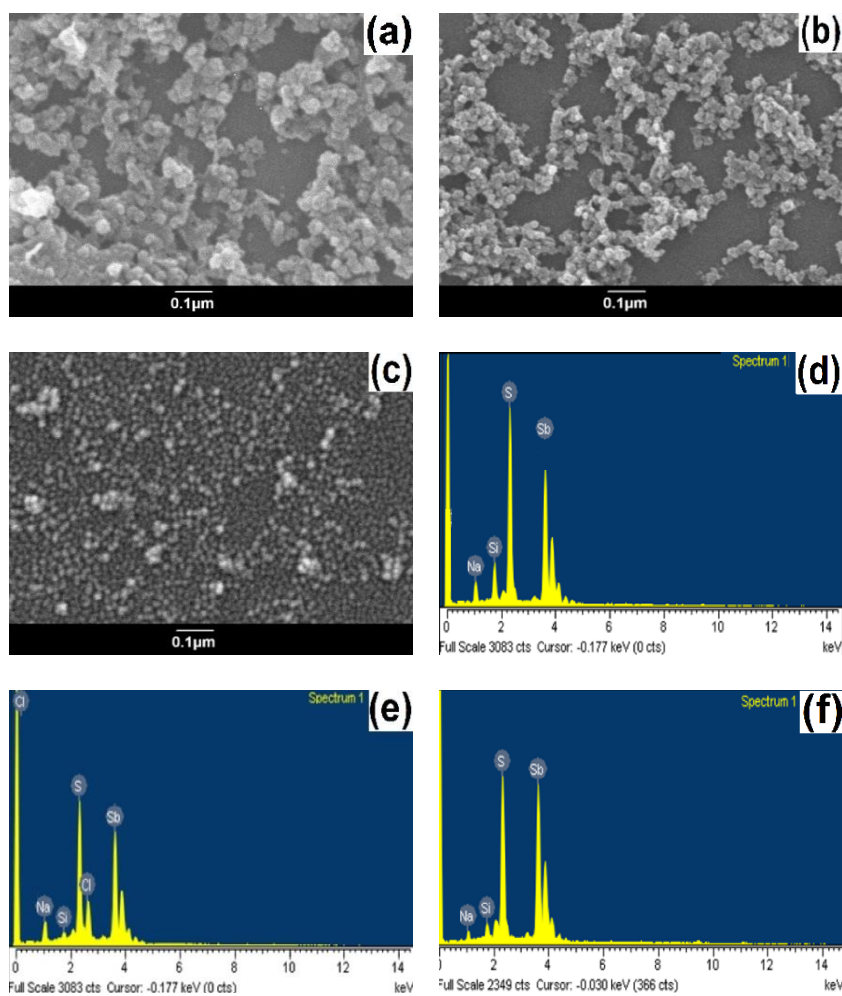


Fig. 2. SEM micrograph of Sb_2S_3 thin films prepared by chemical bath deposition at different temperatures: (a) 0 °C, (b) 5 °C and (c) 10 °C, and the corresponding EDX spectra (d-f).

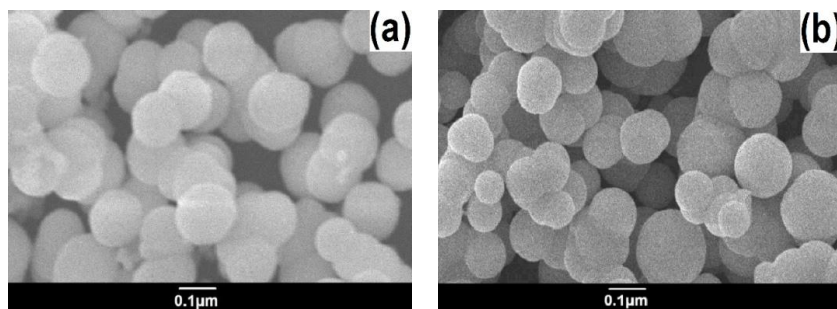


Fig. 3. SEM micrographs of Fe-doped Sb_2S_3 thin films prepared by chemical bath deposition with (a) 3% Fe, and (b) 4% Fe as a dopant.

The SEM micrographs of Fe-doped Sb_2S_3 thin films prepared at 10 °C for 3% Fe and 4% Fe are shown in Fig. 3. The grains are solid and well distributed all over the surface of the films. The crystallite size obtained from SEM images is in the range of 8 to 13 nm. The spherical solid grains with no phase change for higher Fe concentrations suggest that Fe doping in Sb_2S_3 causes reduction in planes as described in XRD discussion.

3.3. RBS analysis

Chemical composition, as well as thickness of the thin films, has been determined by Rutherford Back Scattering (RBS) spectroscopy. The RBS spectra for Fe-doped Sb_2S_3 thin films are shown in Fig. 4.

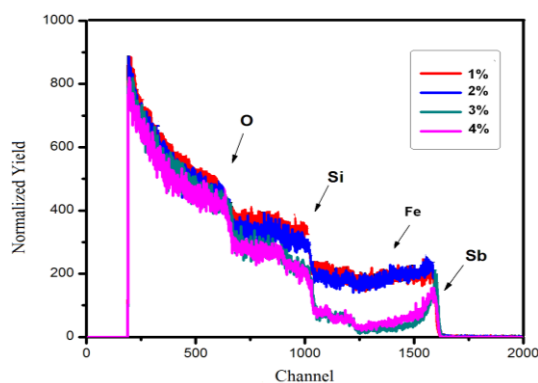


Fig. 4. RBS spectra for Fe-doped Sb_2S_3 thin films prepared at 10 °C.

The small peaks corresponding to “O” and “Si” were due to glass substrate and show that substrate is not uniform and the presence of small edge may be due to the “Sb” and “S” diffusion into the glass substrate. As the film is prepared at low temperature of 10 °C, after annealing no such diffusion is observed. There is no oxide peak which confirms the sulphide formation only. As seen through XRD and SEM analysis the grain growth is on account of Fe doping while uncontrolled growth is observed in case of un-doped thin film. Thicknesses for 1%, 2%, 3%, and 4% Fe-doped Sb_2S_3 thin films were found to be 189.20 nm, 227.3nm, 247.31 nm and 289.79 nm respectively. Structural parameters were calculated from RBS patterns of Fe-doped Sb_2S_3 thin films as well as their atomic percent composition for varying Fe concentrations 1- 4%. The corresponding data is given in Table 4.

Table 4. Thickness and atomic composition of Fe-doped Sb_2S_3 thin films with different Fe concentration in percentage found with RBS technique.

Fe%	Thickness (nm)	Sb (%)	S (%)	Fe (%)
1	189.2	38.57	61.89	1.25
2	227.3	38.01	60.84	2.43
3	247.31	38.81	59.44	3.37
4	289.79	39.02	58.76	3.91

3.4. UV-Visible analysis

In order to study the band structure features of un-doped and Fe-doped Sb_2S_3 thin films, the transmittance versus wavelength measurements were done using UV-Vis spectroscopy operated at normal incidence of light. The optical absorbance spectra of un-doped thin films were recorded in the wavelength range 300 nm to 1000 nm as shown in Fig. 5(a). High absorbance is found in the range 300 – 600 nm, while weak absorbance is observed in the range 600 – 1000 nm. From the figure it is clear that the absorption decreases with the increase of temperature. It is due to the decrease in the particle size as evidenced by the XRD and SEM analysis. The optical band gap of un-doped and Fe-doped Sb_2S_3 thin films was determined using Tauc equation:

$$(\alpha h\nu)^n = A(h\nu - E_g)$$

where $n = 2, 1/2, 2/3$ depend on allowed direct-, allowed indirect-, and forbidden direct transitions respectively, A is constant, h is planks constant and α is the absorption co-efficient which was calculated using:

$$\alpha = \frac{1}{d} \ln \left(\frac{100}{T\%} \right)$$

where d is the thickness of the thin film and ν is frequency. The optical band gap of the films was estimated from the intercept of the straight part of the curves with the horizontal energy-axis.

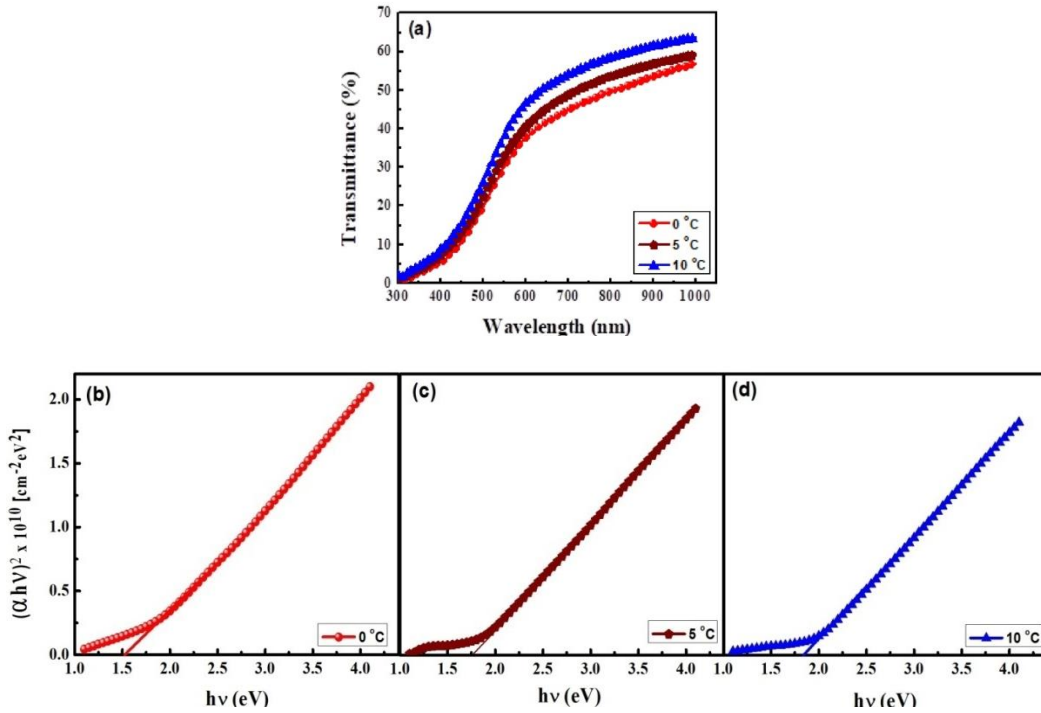


Fig. 5. (a) Optical transmission spectra and (b-d) Tauc plot for the evaluation of band gap energy of Sb_2S_3 films prepared at different temperatures (0 °C, 5 °C, 10 °C) and annealed at 500 °C for 2 hours under N_2 flow.

We have chosen $n = 2$, which gives linear fit for un-doped and Fe-doped Sb_2S_3 thin films. The obtained values of band gap energies for the un-doped Sb_2S_3 thin films prepared at different temperatures of 0 °C, 5 °C and 10 °C and annealed at 500 °C for 2 hours under N_2 flow were in the range 1.53 eV – 1.85 eV (as shown in Fig. 5(b-d)). These values are in agreement with the reported values studied in Ref. [22, 30]. The results show that the band gap increases with the increase of temperature. This may be due to the decrease of number of surface particles forming homogenous thicker films.

The absorption spectra for Fe-doped Sb_2S_3 thin films are shown in Fig. 6 (a) at different percentages of Fe concentration 1% to 4%. The thin films spectra were found in the range of wavelength from 400 nm to 800 nm. It is clear from the spectra that absorbance is similar in both the doped and un-doped samples and shows an overall decrease in absorption with the increase of Fe concentration. A maximum absorption was found in Fe-doped sample in the range of 400–600 nm that is useful in the visible region for electricity generation.

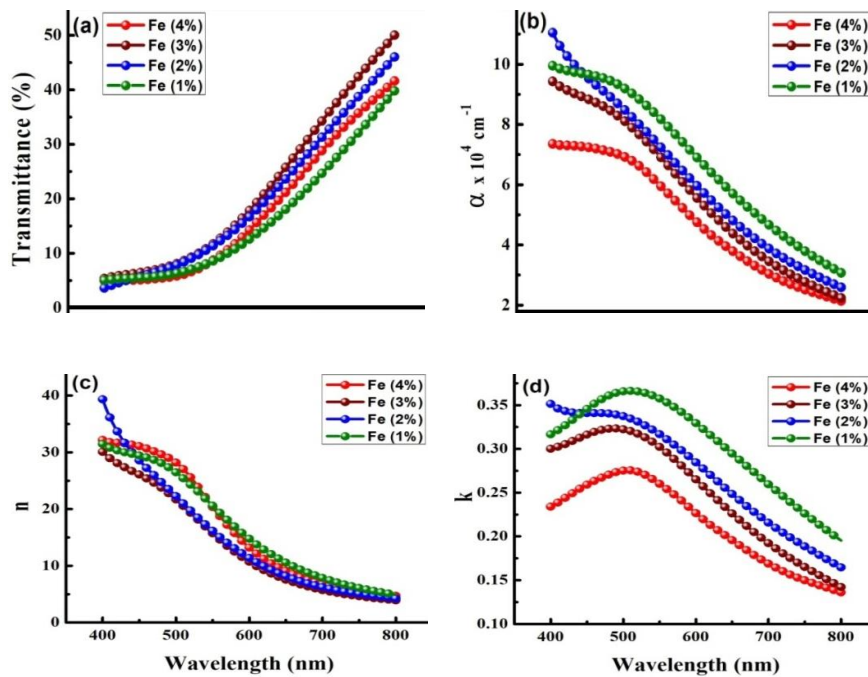


Fig. 6. (a) Optical transmission spectra, (b) absorption coefficient, (c) refractive index, and (d) extinction coefficient plot against wavelength for Fe-doped Sb_2S_3 thin films with varying concentration prepared at 10 °C and annealed at 500 °C for 2 hours under N_2 flow.

The plot of absorption coefficient is shown in Fig. 6 (b). The range of absorption coefficient is $2.1 \times 10^4 - 11 \times 10^4 \text{ cm}^{-1}$ as shown in Table 5. The highest value obtained is $11 \times 10^4 \text{ cm}^{-1}$ for 2 % Fe, and shows almost decreasing trend for higher Fe concentrations. The higher values of absorption coefficients are useful in photovoltaic applications [9, 16].

The refractive index of Fe-doped Sb_2S_3 thin films was calculated using:

$$n = \frac{1 + R}{1 - R} + \sqrt{\frac{4R}{(1 + R)^2} - k^2}$$

The calculated values of refractive index in the range 400 – 800 nm were plotted as shown in Fig. 6(c) The highest value of refractive index shows the improved crystal quality and grain size. The highest value of refractive index is shown by the 2% Fe, and it decreases for all concentrations at higher wavelengths.

The extinction coefficient k was used to find the smoothness and homogeneity of the deposited films[23] by using following relation:

$$k = \frac{\alpha\lambda}{4\pi}$$

The variation of extinction coefficient versus wavelength for doped Sb_2S_3 thin films are shown in Fig. 6 (d). The figure shows an increase in extinction coefficient with the decrease of Fe concentration. All of these concentrations also show a maximum value of extinction coefficient around 500 nm, whereas at higher values of wavelengths its low value shows the smoothness and homogeneity of deposited film.

The optical conductivity was also calculated using:

$$\sigma_o(s^{-1}) = \frac{\alpha nc}{4\pi}$$

Fig. 7 shows that Fe-doped Sb_2S_3 thin films with high optical conductivity response $\sim 10^{15} \text{ s}^{-1}$ in the wavelength range 400 – 800 nm. All the Fe-doped thin films shows similar trend. The optical conductivity decreases with the increase of wavelength and become constant at higher values of wavelengths. Similar result was reported for Sn-doped Sb_2S_3 thin films [16].

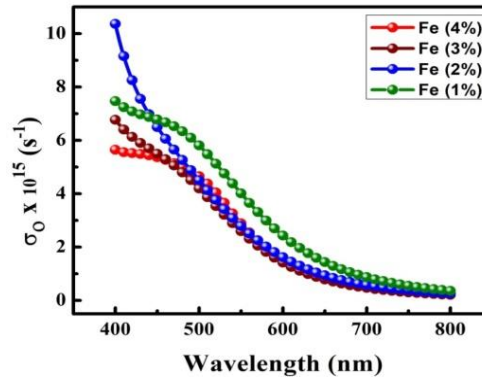


Fig. 7. Optical conductivity variation with wavelength for Fe-doped Sb_2S_3 thin films at various concentrations.

The band gap values for Fe-doped samples were obtained by fitting $n = 2$ in Tauc equation to the experimental data as shown in Fig. 8 (a-d). The band gap values show increasing trend with the increase of Fe concentration. This increase is due to the addition of Fe resulting in the decreasing number of surface particles which consequently forms a homogeneous but slightly thicker film as observed by RBS analysis. This may be due to the new nucleation centers after the Fe doping. The obtained values of the band gap energies lies in the range 1.79 eV – 1.97 eV, which shows the suitability of Fe-doped Sb_2S_3 thin films for the solar cell applications.

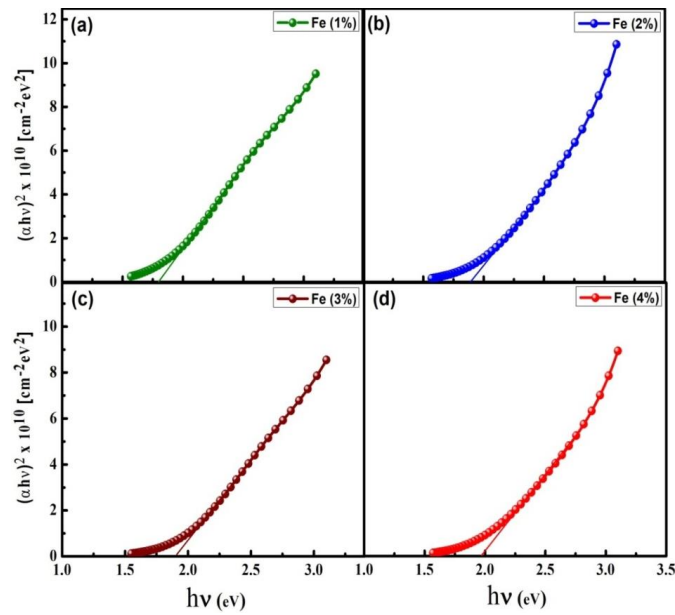


Fig. 8. (a-d) Tauc plot for the evaluation of band gap energy for Fe-doped Sb_2S_3 thin films at various Fe concentrations.

The obtained energy gap values for 3-4 % Fe-doped thin films are higher than those obtained for pure Sb_2S_3 thin film prepared at the same temperature (10 °C) and annealed at 500 °C for 2 hours under N_2 flow. The higher values of the band gap for 3-4% Fe-doped Sb_2S_3 thin films may be due to the crystallinity of the phase obtained, atomic/ weight ratios of elements and interaction of valence band of antimony sulfide with the 3d level of Fe. Similar observations for Sb_2S_3 have been reported in literature where its band gap decreases on Ag doping [30, 37].

4. Conclusions

In this work, the effect of Fe doping on physical properties of Sb_2S_3 thin films has been studied. An optimized temperature of 10 °C was used to obtain a pure crystalline phase for all Fe-doped films. The addition of Fe affects the microstructural properties of the prepared crystalline thin films, i.e., it decreases particle size and increases stresses and dislocation densities. Fe addition to Sb_2S_3 thin films not only improves morphological properties but also interestingly increases the band gap values to lie within the photoactive-visible region. Conclusively one can say that the energy gap values obtained for un-doped and Fe-doped Sb_2S_3 thin films (1.53 eV – 1.85 eV and 1.79 eV – 1.97 eV respectively) are found to be in the range of standard values being used for semiconductors in photovoltaics, which shows high absorbance of the prepared films and hence they can be used as potential candidates for solar cell applications.

Acknowledgement

The authors would like to thank the technical staff at Department of Nano Science and Catalysis Division, National Centre for Physics (NCP), Islamabad, and the Department of Physics, COMSATS University, Islamabad, Pakistan, for helping in the characterization of the samples.

Compliance with Ethical Standards

The authors declare that they have no conflict of interest.

References

- [1] J.Varghese, et al., Nano Letters **12**(2), 868 (2012).
- [2] G.Chen, et al., Journal of Materials Chemistry C **2**(7), 1270 (2014).
- [3] N.Yesugade, C. Lokhande, C. Bhosale, Thin Solid Films **263**(2), 145 (1995).
- [4] F. Aousgi, M. Kanzari, Energy Procedia **10**, 313 (2011).
- [5] O.Savadogo, K. Mandal, Solar Energy Materials and Solar Cells **26**(1-2), 117 (199).
- [6] M.Nair, et al., Journal of The Electrochemical Society **145**(6), 2113 (1998).
- [7] B.Krishnan, et al., Applied Surface Science **254**(10), 3200 (2008).
- [8] F.Aousgi, M. Kanzari, J. Optoelectron. Adv. M. **12**(2), 227 (2010).
- [9] N.Ghraïri, et al., Chalcogenide Letters **7**(3) 217 (2010).
- [10] E.K.Gil, et al., Journal of Nanoscience and Nanotechnology **16**(10), 10763 (2016).
- [11] O.Savadogo, K. Mandal, Journal of The Electrochemical Society **141**(10), 2871 (1994).
- [12] Y.Itzhaik, The Journal of Physical Chemistry C **113**(11), 4254 (2009).
- [13] A.D.DeAngelis, et al., ACS Applied Materials & Interfaces **8**(13) 8445 (2016).
- [14] Y.C.Choi, S.I. Seok, Advanced Functional Materials **25**(19), 2892 (2015).
- [15] A.Blakers, et al., Energy Procedia **33**, 1 (2013).
- [16] S.Mushtaq, et al., Journal of Alloys and Compounds **632**, 723 (2015).
- [17] K.Zhang, et al., Applied Physics Letters **63**(17), 2399 (1993).
- [18] J.Mimila-Arroyo, S. Bland, M. Barbé, Journal of Applied Physics **91**(9), 5923 (2002).
- [19] M.Y.Versavel, J.A. Haber, Thin Solid Films **515**(15), 5767 (2007).
- [20] S.M.Salim, Seddek M. B. Salem, A. M. Islam, Journal of Applied Sciences Research **6**(9), 1352 (2010).
- [21] W.Dong, et al., Thin Solid Films **616**, 80 (2016).
- [22] E.Cárdenas, et al., Solar Energy Materials and Solar Cells **93**(1), 33 (2009).
- [23] S.Mushtaq, et al., Natural Science **8**(02), 33 (2016).
- [24] M.Mitkova, et al., Physica Status Solidi (a) **207**(3), 621 (2010).
- [25] T.Kosa, et al., Journal of Non-Crystalline Solids **164**, 1219 (1993).
- [26] F.Perales, et al., Journal of Physics D: Applied Physics **40**(8), 2440 (2007).
- [27] C.Lokhande, et al., Applied Surface Science **193**(1-4), 1 (2002).
- [28] A.Salem, M.S. Selim, Journal of Physics D: Applied Physics **34**(1), 12 (2001).
- [29] S.Messina, M. Nair, P. Nair, Thin Solid Films **515**(15), 5777 (2007).
- [30] C.Diliegos-Godines, et al., Journal of Materials Science **53**(16), 11562 (2018).
- [31] G.Hodes, Marcel Dekker New York **191**, 2003.
- [32] X.Wang, et al., Journal of Physics D: Applied Physics **39**(23), 4992 (2006).
- [33] H.Maghraoui-Meherzi, et al., Physica B: Condensed Matter **405**(15), 3101 (2010).
- [34] M.Kumar, A. Kumar, A. Abhyankar, ACS Applied Materials & Interfaces **7**(6), 3571 (2015).
- [35] J.Osuwa, N. Osuji, Chalcogenide Letters **8**(9), 571 (2011).
- [36] S.Srikanth, et al., Advances in Science and Research **2**, 95 (2011).
- [37] G.Gong, et al., Applied Catalysis B: Environmental **216**, 11 (2017).